Studies of the Ligand Binding Reaction of Adipocyte Lipid Binding Protein Using the Fluorescent Probe 1,8-Anilinonaphthalene-8-Sulfonate

Jeramia J. Ory and Leonard J. Banaszak
Department of Biochemistry, University of Minnesota, Minneapolis, Minnesota 55455 USA

ABSTRACT The fluorescent probe anilinonaphthalene-8-sulfonate binds to adipocyte lipid binding protein at a site that competes with normal physiological ligands, such as fatty acids. Binding to the protein is accompanied by a relatively large increase in fluorescent intensity. To correlate the major change in optical properties and to determine the mechanism of competitive inhibition with fatty acids, the crystal structure of the protein with the bound fluorophore has been determined. In addition, the thermodynamic contributions to the binding reaction have been studied by titration calorimetry. Because the binding site is in a relatively internal position, kinetic studies have also been carried out to determine k_{on}. The results indicate that binding is not accompanied by any major conformational change. However, the negatively charged sulfonate moiety is not positioned the same as the carboxylate of fatty acid ligands as determined in previous studies. Nonetheless, the binding reaction is still driven by enthalpic effects. As judged by the crystallographic structure, a significant amount of the surface of the fluorophore is no longer exposed to water in the bound state.

INTRODUCTION

Intracellular lipid binding proteins (iLBPs) have the unusual property of having a hydrophobic ligand binding site within a water-filled cavity inside an underlying β-barrel structure. A fluorescent probe, 1-anilinonaphthalene-8-sulfonate (ANS) has been shown to be a competitive inhibitor for binding of the most prevalent ligand, fatty acids (Kane and Bernlohr, 1996; Kurian et al., 1996). ANS is also a commonly used probe employed to observe the character of different regions of globular and membrane proteins (Slavik et al., 1982). Its covalent structure is illustrated in Fig. 1. Crystallographic studies of the bound form of ANS would provide some insight into what binding environment led to changes in ANS fluorescence.

Binding of ANS to several different iLBP family members shows that there is a large fluorescent enhancement accompanied by a blue spectral shift. The binding of ANS to proteins belonging to the iLBP family includes studies of intestinal and adipocyte fatty acid binding proteins, cellular retinol binding protein, and cellular retinoic acid binding protein (*I*). In all of the iLBP family members, the emitted intensity maximum is shifted from 525 nm to ~470 nm (Kane and Bernlohr, 1996; Kurian et al., 1996). For intestinal fatty acid binding protein, the ratio of the quantum yield for the bound versus free ANS in aqueous solution is of the order of 160 (Kirk et al., 1996). Recognizing some small variation, the fluorescent enhancement experienced by the fluorescent probe appeared to be similar for the fatty acid and retinoic acid binding proteins, but was reduced by ~½ for the cellular retinol binding protein.

The two binding studies mentioned above established the stoichiometry as one ANS per iLBP molecule (Kane and Bernlohr, 1996; Kurian et al., 1996). Since the binding cavity for the fatty and retinoic acid binding proteins contains two buried arginines that interact with the carboxylate of the hydrophobic ligands, it is reasonable to expect the sulfonate moiety of ANS to locate near these arginine side chains. In the retinol binding proteins, where the ligand is neutral, these two internalized arginine sites are present as glutamines (Banaszak et al., 1994). ANS still binds to cellular retinol binding protein, but with a lower affinity and a reduced fluorescent enhancement.

The dissociation constants for ANS binding to the fatty acid binding proteins ranged from ~500 nM to 5 μM. In the case of intestinal fatty acid binding protein, ANS binding was also studied by isothermal titration calorimetry (Kirk et al., 1996). The K_D values determined by the two methods were in general agreement. The calorimetric analysis produced a value for ΔH and indicated that most of the binding energy was derived from the enthalpic contribution. The chemical studies also demonstrated that the binding of ANS to the iLBPs competes with fatty acid binding. This then suggests that the location of the ANS binding site is within the cavities of the iLBPs. The competitive nature of ANS binding also made it possible to study fatty acid affinity (Kane and Bernlohr, 1996; Kurian et al., 1996).

While the use of ANS as a conformational probe continues to increase, few detailed structural data are available on the factors contributing to the changes in fluorescent properties. A single crystallographic study describes the binding of ANS to α-chymotrypsin in both solution and crystalline environments (Weber et al., 1979; Johnson et al., 1979). The fluorescent enhancement for ANS bound to α-chymotrypsin appears to be similar to that observed upon binding to the

Received for publication 28 January 1999 and in final form 3 May 1999.

Address reprint requests to Dr. Leonard J. Banaszak, Department of Biochemistry, Molecular Biology and Biophysics, University of Minnesota, 4-225 Millard Hall, 435 Delaware St. S.E., Minneapolis, MN 55455. Tel.: 612-626-6597; Fax: 612-624-5121; E-mail: len b@dcmir.med.umn.edu.

Jeramia J. Ory's current address is Department of Biochemistry and Molecular Biophysics, Washington University Medical School, 660 S. Euclid Avenue, Box 8231, St. Louis, MO 63110.

0006-3495/99/08/1107/10 $2.00

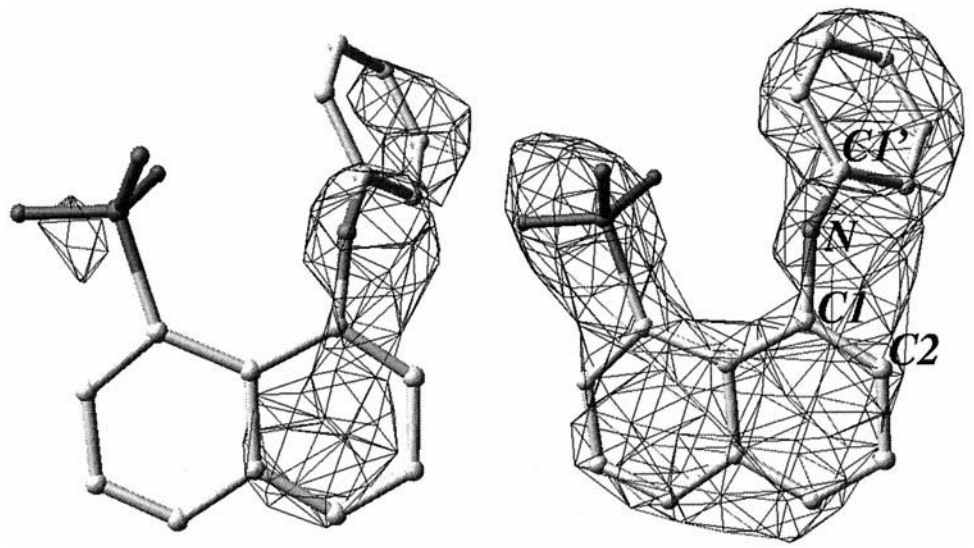

FIGURE 1 Electron density maps of ANS. A simulated annealing omit map (*left*), and final omit map (*right*), both contoured at 3σ, illustrating the initial ambiguity of the maps. The C1′–N–C1–C2 atoms are labeled for reader reference, especially to Table 2.

iLBPs, but was strongly pH-dependent (Weber et al., 1979). The crystal structure demonstrated that ANS was bound at a surface site. In this unrefined crystallographic study of the chymotrypsin complex, the aniline-ring was approximately coplanar with that of the naphthalene moiety (Weber et al., 1979).

The quantum yield and fluorescent lifetime of a bound fluorophore are highly dependent on the absence of nonradiative transitions (Slavik et al., 1982). The very high quantum yields for ANS bound to adipocyte lipid binding proteins (ALBP) and intestinal fatty acid binding protein (IFABP) suggest that the pathways of energy transfer through excited state interactions have been limited, most likely by a partial occlusion of the ANS from bulk solvent. In the crystallographic analysis that follows, the conformation and interactions of ANS with the protein ALBP are analyzed in detail. The ALBP crystals contained two molecules per asymmetric unit and a comparison between the conformations of the two ANS molecules will be given. Additionally, a comparison between the ANS conformations as bound to chymotrypsin and ALBP will be made. Finally, characterization of the ALBP/ANS reaction using isothermal titration calorimetry and stopped flow kinetics will be presented. The kinetic results proved complex, and could not be explained by a pseudo-first-order reaction.

MATERIALS AND METHODS

Expression, purification, and preparation of co-crystals

Native murine ALBP was expressed and purified as previously reported (Xu et al., 1991). Pure ALBP was concentrated to ~10 mg/ml in 12.5 mM HEPES pH 7.2, 50 mM NaCl. The NH_4^+ salt of ANS was dissolved in 12.5 mM HEPES pH 7.2, 50 mM NaCl, and the concentration verified spectrophotometrically (ϵ_{280} = 4990 M^{-1} cm^{-1}). This ANS stock was added to the ALBP solution so a 2:1 ANS/ALBP stoichiometry was achieved without significant dilution of the ALBP. The incomplete factorial and novel matrix methods of crystallization screening were employed (Carter and Carter, 1979; Jancarik and Kim, 1991) using the vapor-diffusion/hanging drop procedure. Crystals formed at 0.1 M HEPES pH 7.5, 2% v/v PEG 400, and 2.0 M $(NH_4)_2SO_4$.

X-ray methods

X-ray diffraction data were collected at room temperature on a Siemens multiwire area detector, with CuK_α radiation from a Rigaku RU-200 generator equipped with a graphite crystal monochromator. Data were collected with a crystal to detector distance of 11.7 cm and a crystal rotation of 0.25° between frames. Data collection statistics are reported in Table 1. The XENGEN suite of programs was used to process the initial data and determine the space group.

Model refinement

Starting phases were derived from the coordinates obtained from an isomorphous crystal form of ALBP modified with a pyridoxamine group (Ory et al., 1998). Coordinates of the pyridoxamine moiety were removed, and further refinement of the structure was carried out in X-plor (Brunger et al., 1987), with initial rigid body refinement being followed by simulated annealing (Brunger, 1988). Multiple rounds of positional and B-factor refinement were accomplished using a bulk-solvent correction (Jiang and Brunger, 1994). The ANS was added to the structure and fit to both $2|F_o|-|F_c|$ maps contoured at 1σ and $|F_o|-|F_c|$ maps contoured at 3σ. Waters were placed in the model late in refinement, and had to be present in both $2|F_o|-|F_c|$ maps contoured at 1σ and $|F_o|-|F_c|$ maps contoured at 3σ. The water sites were required to be between 2.5 Å and 3.5 Å away from a proper hydrogen bond donor/acceptor atom. The R_{factor}/R_{free} was monitored at all stages in refinement to ensure proper fitting and building of the model (Brunger, 1992). Final refinement statistics are presented in Table 1. All cavity volume measurements were calculated using the algorithm CAST (Liang et al., 1998) and manually inspected for cavity continuity. For cases where NMR structures existed, all volumes of all reported structures were averaged, and standard deviations reported.

Stopped-flow measurements of ALBP/ANS reaction

Kinetic data for the binding reaction were collected on an Applied Photophysics SX.18MV stopped-flow reaction analyzer interfaced to an Acorn

TABLE 1 X-ray data and refinement results of crystalline ALBP/ANS complex

Variable	Refinement	
Range	24–2.5 Å	2.7–2.5 Å
Collected reflections	74950	3176
Unique reflections	12287	1263
R_{merge}	10.2%	31.2%
Space group	$P2_12_12_1$	
Unit cell (a × b × c)	80.8 Å × 96.1 Å × 49.9 Å	
Completeness ($I/\sigma I > 1.0$)	95%	58%
Molecules per asymmetric unit	2	
Refinement results		
Number of atoms		
protein	2034	
water	78	
ligand	42	
nonwater het-atoms	1 Cl^- ion	
R_{factor}/R_{free}	18.9%/24.7%	
B factors (avg.)		
main chain	24.1 $Å^2$	
side chain	26.6 $Å^2$	
ligand (ANS)	73.8 $Å^2$	
waters	36.5 $Å^2$	
RMS bond length (Å)	0.007	
RMS bond angle (deg)	1.581	
Overall G-factor	0.2	
Bad contacts	0	

RiscPC. Both protein and ligand samples were in 20 mM Na^+/K^+ phosphate buffer, pH 7.2, and their concentrations verified spectrophotometrically. ALBP was delipidated before data acquisition by treating with Lipidex resin at 37°C using a batch method. For the stopped-flow study, the protein syringe contained ALBP in phosphate buffer at 10 μM, with the ligand syringe containing increasing amounts (40, 60, 80, 100, 200, 300, 400, 500, 600, and 700 μM) of ANS in phosphate buffer. ANS fluorescence was monitored using an excitation wavelength of 380 nm and an emission wavelength of 475 nm. Voltage to the photomultiplier was held constant throughout the data acquisition, and all runs adjusted to a common endpoint to account for native ANS fluorescence. This was verified independently with ANS and buffer alone for initial runs. Runs were collected five times over a logarithmic time scale and averaged by the data collection software. Initial runs were carried out at 25°C, but it was observed that the majority of the reaction was complete (~75% of the calculated maximal amplitude change) in the dead time, even at the lower ANS concentrations. The runs were then repeated at 4°C to better observe the fastest process. All runs were carried out in dim light conditions, and solutions were allowed to equilibrate to 4°C before data acquisition.

Data manipulation of stopped-flow results

The raw data were shifted by the dead time of ~2 ms (Tonomura et al., 1978). The data were fit to one, two, and three exponential equations using KFIT (Neil Millar, ftp://wuarchive.wustl.edu/packages/kinsim/uploads). The KINSIM (Dang and Frieden, 1997) suite of programs and KSIM (Neil Millar) were used to test potential models and fit the data. The reaction was assumed to start at the same zero time point for fitting to all equations. This was done to accommodate the observance that more and more of the fastest reaction disappeared in the dead time of the instrument as ligand concentration increased.

Isothermal titration calorimetry of the ALBP/ANS reaction

Calorimetric analysis was carried out on a Microcal (Northampton, MA) calorimeter. 35.5 μM ALBP in 20 mM Na^+/K^+ phosphate buffer, pH 7.2, cell volume 1.3438 ml, was titrated with 15-μl injections of 439 μM ANS in the same buffer using 15 s per injection and a stirring rate of 400 rpm. All titration runs were followed with reference runs of 439 μM ANS injected into buffer alone. The reference runs were then fit to a linear function, and the line subtracted from the raw data to account for heat of dilution and temperature differences between the injection syringe and the bath. Protein and ANS concentrations were verified spectrophotometrically before data fitting, as the enthalpy of binding and the stoichiometry of the reaction is sensitive to the ligand concentration used to fit the data. The raw data were integrated and processed with the Origin 2.9 suite of programs.

RESULTS

Crystallographic analysis of ALBP/ANS complex

General characteristics of the crystallographic data and model results are given in Table 1. As indicated by the value for R_{merge}, multiple measurements of the same reflections agreed within a satisfactory range. The resolution extended to 2.55 Å and was 95% complete with an overall $I/\sigma I$ value above 1.0. As mentioned in the Methods section, the phases were obtained from an isomorphous structure [pdb1a2d.ent in the Protein Data Bank (PDB)]. An $|F_o|$-$|F_c|$ map was not useful, as the isomorphous structure contained a chemical adduct that partially filled the binding cavity, possibly biasing electron density in the region of ANS. Nonetheless, electron density for the ANS was present during all stages of refinement, but was ambiguous in both the $2|F_o|$-$|F_c|$ and $|F_o|$-$|F_c|$ maps. To eliminate ambiguity, the ANS was modeled initially in two conformations within the cavity and refinement carried out in parallel on both structures. After refinement, the shape of the resultant electron density was the same regardless of initial ANS orientation. This new electron density map clearly favored one conformation over the other. Simulated annealing and final omit maps of the ANS group are shown in Fig. 1. Though the electron density is noncontiguous in the simulated annealing omit map contoured at 3σ, it is clearly visible and contiguous when contoured at 2σ (data not shown).

After refinement, all of the atoms in the ALBP polypeptide chain were accounted for as well as the presence of bound ANS, 1 Cl^-, and 78 water molecules. Since there are two molecules in the asymmetric unit, a crude approximation to the precision of the coordinates is apparent from the RMS difference after superimposing one molecule on another. For C_α atoms, the RMS difference was 0.22 Å, and 0.96 Å RMS difference using all atoms. The resolution limit of the data was judged to be of sufficient quality not to enforce noncrystallographic symmetry restraints to the refinement protocol. The crystallographic coordinates for the ANS/ALBP complex have been deposited in the PDB with the accession code 2ANS.

The crystallographic results reveal the ANS ligand bound within the cavity normally occupied by fatty acids. The

overall positioning of ANS relative to the C_α backbone model of ALBP is illustrated in Fig. 2. Essentially identical results are obtained independent of which of the two protein molecules in the crystal are observed. Note in Fig. 2 that all of the atoms of the ligand are within the strands of the ALBP β-barrel. Fig. 2 also contains a ball-and-stick representation of the long-chain sulfonate, hexadecane sulfonic acid (HDS), obtained from a different crystallographic analysis (LaLonde et al., 1994a). The coordinates of HDS were placed in the crystallographic coordinates of the ANS-ALBP complex using least-squares methods. Note that a number of the atoms belonging to ANS are in similar positions to those belonging to a fatty acid ligand.

Despite clear overlap between the binding site for ANS and previously determined positions for fatty acids, the ANS site is in a significantly different orientation. Essentially, it is "flipped" from the orientation that we expected it to adopt with the negative sulfonate headgroup pointing more toward the portal region. This is the area capped by the βC-βD and βE-βF loops and helix αII. It is the aniline ring of ANS that interacts with the normal carboxylate binding pair of R126/Y128.

Because of the substantial fluorescent enhancement of bound ANS, the protein conformation near the ANS in the crystal structure has been studied in detail. The two molecules in the asymmetric unit were analyzed for van der Waals and potential polar contacts using the program HBPLUS (McDonald and Thornton, 1994). The principal contacts are shown schematically in Fig. 3. Numerous hydrophobic contacts with the ANS are made in both molecules, including an edge-to-face interaction of Phe-16 to the naphthyl ring of ANS.

Similar to what was observed in the crystal structure of α-chymotrypsin/ANS (Weber et al., 1979), the interactions are not strictly hydrophobic. This is not surprising, as the cavity of ALBP is lined with approximately an equal number of polar and hydrophobic amino acids, and it would be difficult for any ligand to make a "strictly hydrophobic" interaction. Some of the interactions, however, are unusual. Perhaps most striking is the relatively close interaction of the benzyl ring of Phe-57 with a sulfonate oxygen of the ANS. To make this interaction, the main chain of Phe-57 moves 1.87 Å and 2.6 Å toward the binding cavity when compared to the native-apo or oleate-bound structures of ALBP, respectively.

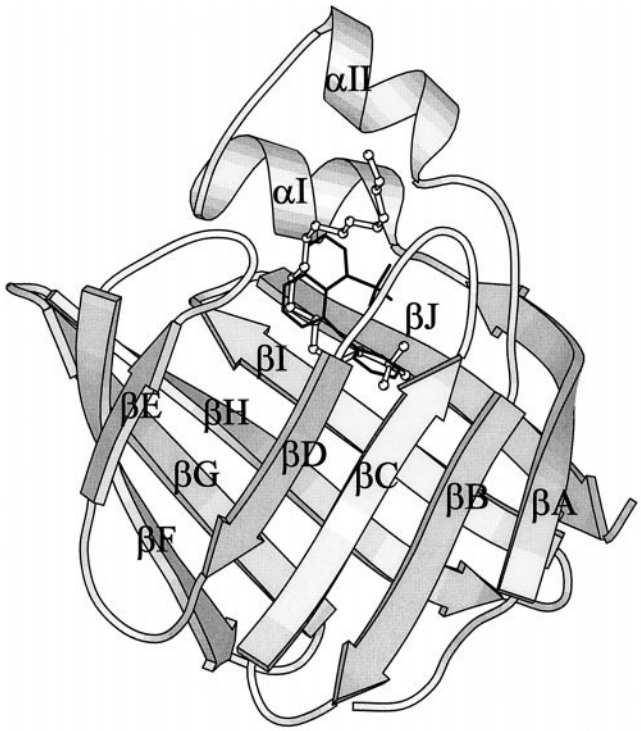

FIGURE 2 Binding mode of ANS. A cartoon representation of the crystal structure of ALBP/ANS. ANS is represented as blackened bonds. The structure of hexadecanesulfonate (HDS)-bound ALBP (pdb1lic.ent) was superimposed with the ANS bound structure, and the resultant coordinates for HDS shown as a ball-and-stick. Elements of secondary structure are labeled for reader reference. The portal region is the area between helix αII, the βC-βD turn, and the βE-βF turn.

Thermodynamic analysis of the ALBP/ANS reaction

By using isothermal titration calorimetry, the enthalpy of binding was measured at nine different temperatures, and the free energy and entropy of binding calculated using the following equations: $\Delta G = -\mathrm{RTln}(K_a)$, $\Delta G = \Delta H - T\Delta S$. The results were then used to compute the heat capacity changes for the binding reaction. The results are given in Table 4. The data used to determine the heat capacity are shown in Fig. 4. The binding reaction had a ΔC_p, -220.3 ± 13.4 cal/deg-mol.

The values at 30°C given in Table 4 for ALBP ($\Delta G = -8.0$ and $\Delta H = -9.6$ kcal/mol) can be compared to a similar study by Kirk et al. (1996) utilizing IFABP. Using titration calorimetry, ANS bound to IFABP had a K_d of 11.4 μM at 30°C. The binding reaction for ANS to IFABP gave values of -7.1 kcal/mol for ΔG and -10.5 kcal/mol for ΔH. The thermodynamics are clearly very similar, and therefore the binding reactions and probably the fluorescent enhancement to both ALBP and IFABP appear to be comparable. Since they are homologous proteins, this is not surprising. However, the binding cavity of IFABP is smaller than ALBP, which may have some bearing on understanding the structural determinants of the interaction and will be discussed in more detail in the Discussion section.

Kinetic analysis of the ALBP/ANS reaction

To further characterize the ligand binding reaction, stopped-flow analysis was performed to determine the reaction rates. The kinetic studies were carried out at varying concentrations of ANS, and the raw data are shown in Fig. 5 *D*. The kinetic data did not satisfactorily fit to a single or double exponential (data not shown), but were adequately repre-

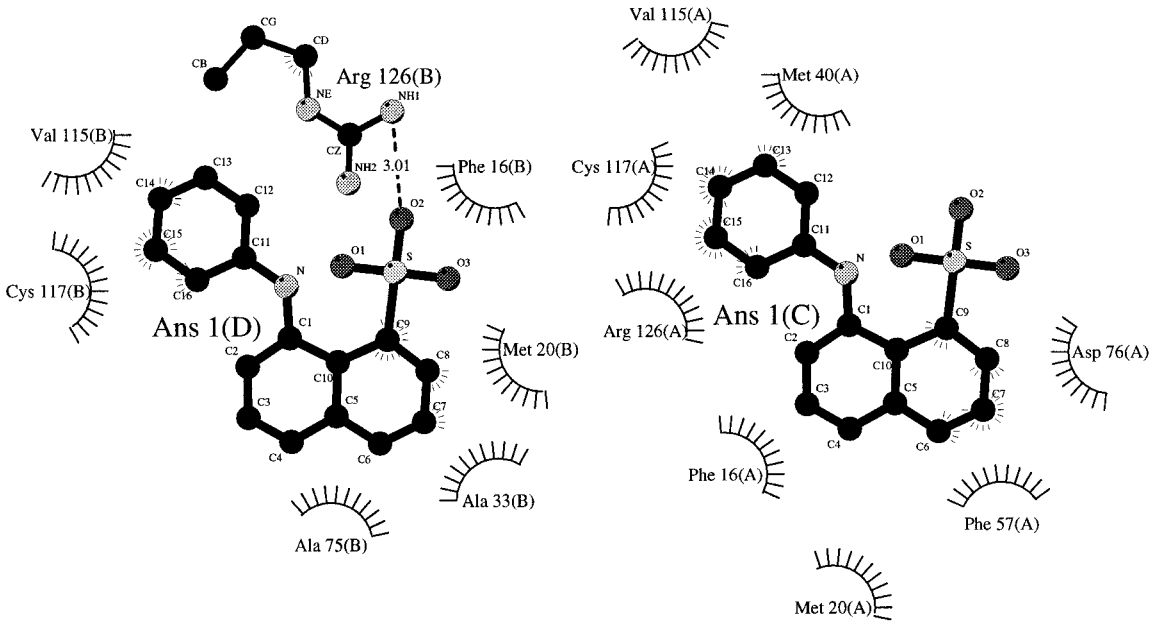

FIGURE 3 ANS interaction sites on ALBP. Principal interaction sites between ANS and ALBP are shown schematically. Two sites are displayed representing the two ALBP molecules found in the asymmetric unit of the crystalline complex. The spikes emerging from both protein and ligand atoms denote nonpolar contacts. The interaction between R126 and an oxygen atom of ANS is near the limit of detection of the searching algorithm for one of the ALBP molecules, and therefore appears in only one molecule, ANS 1(D). The analyses and drawing were done with LIGPLOT.

sented by a three-exponential function. As a result of this analysis, plots of the three relaxation times as a function of ANS concentration are shown in Fig. 5, *A–C*.

The three-step interpretation results in the fastest step (Fig. 5 *A*), being pseudo-first-order with respect to ANS. The second reaction (Fig. 5 *B*) is again pseudo-first-order with respect to ANS, but is slower by a factor of ~25. The slowest step is zero order with respect to the fluorescent probe concentration, as is apparent in Fig. 5 *C*.

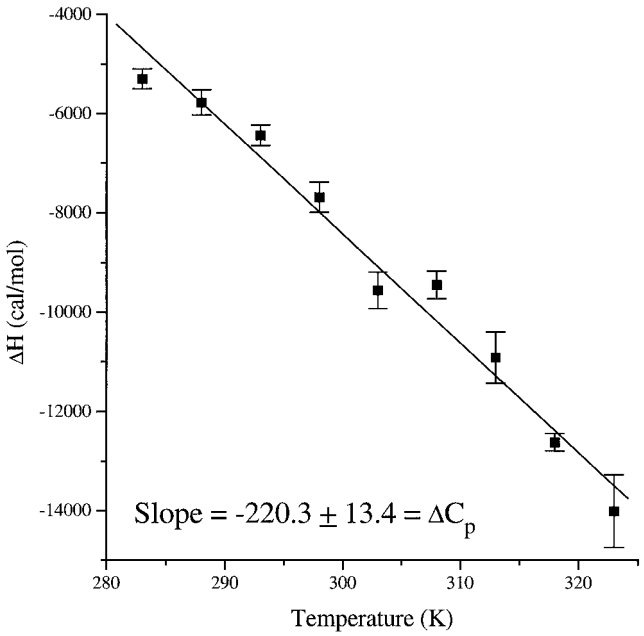

FIGURE 4 Determination of specific heat capacity of the ALBP/ANS reaction. The enthalpy of the binding reaction is plotted as a function of temperature. The error bars indicated at each measurement are the result of errors in fitting a standard binding isotherm to the data obtained from the calorimeter.

DISCUSSION

The fluorescent enhancement accompanying ANS binding to ALBP has been observed to varying degrees with many proteins. The only other crystallographic study examining the nature of protein interactions with this fluoroprobe involved ANS bound to α-chymotrypsin. Weber et al. (1979) found in solution and in the co-crystal that ANS bound to α-chymotrypsin, but showed fluorescence enhancement only when the pH dropped below 3.6. The crystal structure of the ANS-bound complex was solved at both pH 3.6 and pH 7, and the structure of the ANS analyzed. No pH-dependent conformational change was found either in the protein environment surrounding the ANS or in the ANS itself. The authors mention that a structural change is seen in α-chymotrypsin below pH 5.0, but do not expand on this finding, nor relate it to ANS binding or fluorescence. Assuming the structural change is not near the ANS binding site, this would suggest the fluorescent enhancement is due to the change in protonation state of the bound ANS and the different interactions available to the protonated form.

The chymotrypsin study was done before the establishment of the Brookhaven structural database and before modern x-ray refinement methods, so no coordinates for the protein-ANS complex are available from the study. The authors did list the coordinates of the ANS alone when

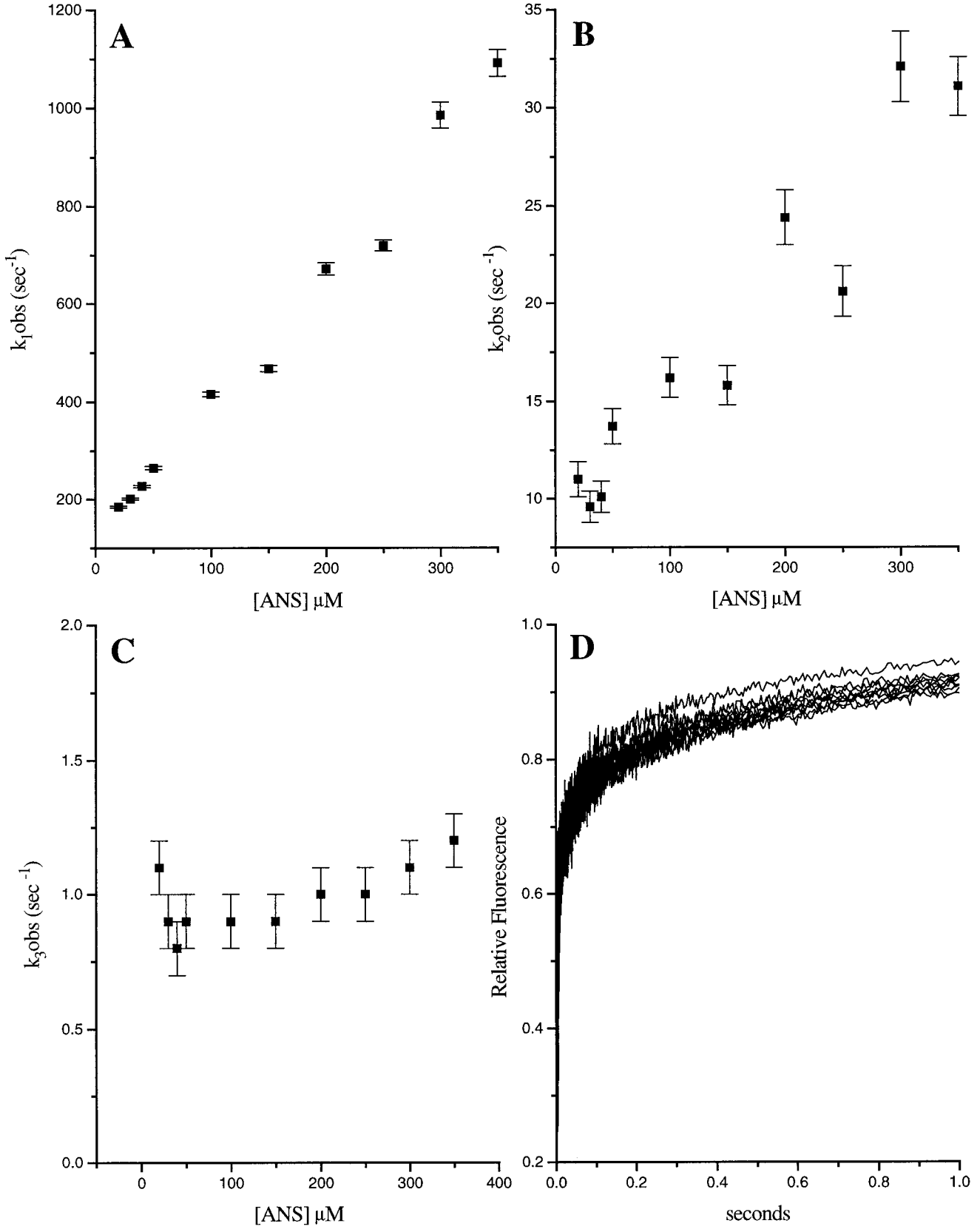

FIGURE 5 Relaxation times of the ALBP/ANS reaction. Raw stopped-flow data (*D*) were fit to a three-exponential equation, and observed rate constants plotted as a function of final ligand concentration (*A–C*). Error bars represent errors of fitting.

bound to α-chymotrypsin. We have used them to compare the structure of ANS bound to chymotrypsin, to ALBP, and the crystal conformation of ANS itself. Two angles may be used to describe most of the conformation of the ANS; they are listed in Table 2. The values of α (dihedral angle between the naphthyl and anilino ring) and the torsional angle defined by C11–N–C1–C2 are reported. The values for molecule A in the small molecule study is roughly similar to the two values of these angles when the ANS is bound to ALBP and to ANS alone, as described in the Weber and Tulinsky report. The similarity between the bound and unbound conformations suggests that the fluorescent enhancement found on binding to a protein is not related to the conformation of the fluorophore, but rather the energy pathways available between the excited state and its surroundings, chiefly bulk solvent.

With α-chymotrypsin, ANS binds to a surface site; in binding to ALBP, it is located within a cavity. To see whether any detectable changes occurred, the cavity volumes of both ALBP molecules were calculated using the CAST algorithm (Liang et al., 1998). These data were then compared to all previously solved structures of ALBP, including studies of the protein with long-chain fatty acids, and the results are shown in Table 3. Volume calculations have suggested increases in cavity volume as a result of ligand binding to iLBPs (LiCata and Bernlohr, 1998). In the case of the crystal structure of the ANS/ALBP complex, no such expansion occurs. The cavity volumes of apo-ALBP and ANS bound to ALBP are almost identical, perhaps somewhat smaller. Hence, the relatively small volume expansion observed with ALBP and other iLBPs and accompanying fatty acid binding does not occur with ANS. This means that the number of internalized solvent molecules is approximately the same for complexes of ALBP with the fluoroprobe and more physiological ligands such as fatty acids.

The crystal structure of ANS bound to ALBP reveals an unusual and previously unseen ligand-binding mode for the iLBP family. The negatively charged headgroup of ANS, instead of being coordinated by the R106/Y128/R126 binding triad, interacts with mostly hydrophobic side chains inside the cavity. The only ionic interaction is a weak electrostatic bond between a terminal nitrogen atom of R126 and an oxygen atom of the sulfonate moiety ~3.1 Å away. While the binding mode is unusual, it may be due to the nature of the ligand. This structure is the first of its kind with a significant aromatic component bound to a member of the iLBP family.

TABLE 2 Angles defining ANS conformations

ANS Structure	C11–N–C1–C2	α*
ALBP ANS A[#]	78°	64°
ALBP ANS B[#]	76°	57°
α-CHT ANS A[#]	10°	NR[§]
α-CHT ANS B[#]	−27°	NR[§]
Weber & Tulinsky	43°	61°
Cody & Hazel A[#]	22°	63°
Cody & Hazel B[#]	−46°	127°

The C11–N–C1–C2 angle is a torsional angle. See Fig. 3.
*Defined as the dihedral angle between the plane of the anilino ring and the plane of the naphthyl ring.
[#]A and B indicate more than one conformation, or more than one molecule per asymmetric unit. Weber and Tulinsky, and Cody and Hazel derived the angles from the crystal structures of unbound ANS.
[§]Not reported due to spherical averaging of density.

TABLE 3 Volume comparisons for the ALBP ligand-binding cavity

Protein	Comment	Volume (Å^3)	Average
ALBP			
1ALB	Apo	1039.4	1005.35 ± 48.2
1LIB	Apo	971.3	
1LIC	Hexadecanesulfonate	1096.4	1113.3 ± 18.2
1LID	Oleate	1125.8	
1LIE	Palmitate	1108.5	
1LIF	Stearate	1092.0	
1ADL	Arachidonate	1133.8	
1AB0	Mutant, pH 4.5	1016.8	1169.3 ± 215.6
1ACD	Mutant, pH 6.4	1321.7	
ANS-A	ANS, Mol A	932.2	908.4 ± 33.6
ANS-B	ANS, Mol B	884.6	

The volumes were calculated with the CAST algorithm, and visually inspected for continuity (Liang et al., 1998). All volumes are the "Vol ms" from CAST. They represent a volume "cast" from molecular surface of the crystal structure of ALBP without any ligand.

A comparison of the ANS/ALBP crystal structure with coordinates for other complexes of ALBP was done. It is immediately obvious that ANS and a fatty acid ligand could not occupy the ligand-binding cavity at the same time; considerable atomic overlap exists between portions of the bound ligands (the reader is referred to Fig. 2). It is also apparent that the location of the sulfonate of ANS and the carboxylates of fatty acids is different. The crystallographic studies indicate that ANS and fatty acid ligands "partially compete." The negative aspect of the structural results is that dissociation constants determined for fatty acid binding by competition with ANS are technically inhibitory constants (K_i), not dissociation constants. They will rely heavily on accurate determination of the binding constant of the ALBP/ANS reaction.

To further explore the binding reaction, isothermal titration calorimetry was used on the ALBP/ANS reaction to determine ΔH and K_d. The results are given in Table 4. The reaction is entropically opposed above 25.0°C, but this effect is compensated for by a large enthalpy of binding at higher temperatures. This higher enthalpy is a bit unusual due to the lack of any significant ionic interaction similar to those seen for fatty acids. This may call for a slight reevaluation of the binding energy terms of the binding reaction for physiological ligands. LaLonde et al. (1994b) suggested that the majority of the favorable enthalpic binding energy stems from the coulombic interactions of the negative fatty acid headgroup with the positive groups R126 and a water-bridged R106. ANS, however, has an interaction with R126

TABLE 4 Thermodynamic parameters for the ALBP/ANS reaction

Temp. (°C)k	k_d (μM)	ΔG (kcal/mol)	ΔH (kcal/mol)	ΔS (e.u.)
10.2	1.9 ± 1.0	−7.4 ± 0.12	−5.3 ± 0.20	7.4 ± 0.8
15.1	1.4 ± 0.9	−7.7 ± 0.14	−5.8 ± 0.25	6.6 ± 1.0
20.1	1.0 ± 0.6	−8.0 ± 0.14	−6.4 ± 0.21	5.4 ± 0.8
25.1	1.2 ± 0.8	−8.1 ± 0.16	−7.7 ± 0.30	1.3 ± 1.1
30.2	1.7 ± 1.0	−8.0 ± 0.14	−9.6 ± 0.37	−5.1 ± 1.3
35.1	1.5 ± 0.7	−8.2 ± 0.12	−9.5 ± 0.28	−4.0 ± 1.0
40.1	1.6 ± 1.2	−8.3 ± 0.18	−10.9 ± 0.52	−8.4 ± 1.8
45.1	2.1 ± 0.4	−8.3 ± 0.05	−12.6 ± 0.17	−13.7 ± 0.6
50.1	2.2 ± 1.7	−8.3 ± 0.19	−14.0 ± 0.74	−17.6 ± 2.4

The parameters of the binding reaction for temperatures in the range of 10 through 25.1°C were measured with a bath temperature of 5.0°C. For the studies in the temperatures range of 30.2°C through 50.1°C, a bath temperature of 25.0°C was used. All values are based on a single experiment and the errors are estimated from the titration data using the Origin 2.9 program. The K_D values are based on the stoichiometry of one ANS site per ALBP molecule.

that is weak at best, makes extensive nonpolar contacts with the binding cavity, and yet has a very high enthalpic contribution. Regardless, the thermodynamic binding profile for ANS is similar to that of other ligands, being driven mostly by a highly favorable enthalpic energy that is offset by unfavorable entropy at physiological temperatures.

The large negative heat capacity seen for the ALBP/ANS reaction is consistent with results seen in the binding of ANS to a homologous protein, IFABP. The calculated ΔC_p for the ALBP/ANS reaction is ~−220 cal/deg-mol, while the ΔC_p for the IFABP/ANS reaction is ~−283 cal/deg-mol (Kirk et al., 1996). Furthermore, the overall thermodynamic profile is similar for IFABP bound to ANS; the IFABP/ANS reaction is entropically opposed above 15°C, while the ALBP/ANS reaction is entropically opposed above 25°C. Kirk et al. suggest that this negative change in the heat capacity in the case of IFABP is due mostly to the loss of internal hydrogen bonds of waters found in the cavity that are displaced by the ligand (Kirk et al., 1996). The authors further suggest the degrees of freedom available to cavity waters are fewer when ligand is bound, helping to increase the entropic opposition. Unfortunately, current structural work offers no insight into this possibility.

Comparison of the apo-ALBP structure (1LIB in the PDB) to the ALBP/ANS structure reveals one crystallographically ordered water in the apo state that would theoretically be displaced by ANS binding. The binding of any ligand must displace more than one water molecule. However, the lack of ordered water molecules observed in the ANS region in other ALBP crystal structures suggests that water molecules in this area of the cavity are more highly exchangeable. The entropic opposition to binding can also be explained if the dominant part of ΔS is due to ANS and its more rigid conformation when bound to the protein than when free in solution.

After verifying that ANS could be used as an accurate measure of the ligand binding reaction, the fluorescent properties of ANS were exploited to explore the kinetics of the binding reaction. Since the static model of ALBP has the binding site within a cavity, various ideas have been offered as to the mechanism of binding. The best way to study the native ligand binding reaction would be to monitor native tryptophan fluorescence transiently in response to added fatty acid, as was done in the case of IFABP (Cistola et al., 1996). However, previous studies have shown little to no change in the native tryptophan spectra of ALBP in response to various fatty acids (Bernlohr and Simpson, personal communication). Instead, the ALBP/ANS reaction was followed using stopped-flow methods.

Interestingly, the stopped-flow data exhibited behavior that suggested a complex binding mechanism consisting of two relaxation times dependent on ANS concentration (k_1^{obs} and k_2^{obs} in Fig. 5, *A* and *B*), with an event whose relaxation time was most likely not dependent (k_3^{obs} in Fig. 5 *C*) on the ANS concentration. The number of reaction mechanisms that may accommodate three reaction times is great. That being said, previous biochemical evidence can help to rule out most mechanisms. Two ligand-dependent relaxation times could be indicative of two binding sites. However, isothermal titration calorimetry and crystallography clearly show a binding stoichiometry of one, and so the second site would have to be extremely weak (in the mM range). Furthermore, all reaction mechanisms that incorporated irreversible steps were eliminated, as the binding constant is not strong enough (~1 μM) to be treated as such, nor has any part of this reaction been shown to be irreversible.

Attempts to globally fit the kinetic data to numerous other models were unreliable. This is primarily due to the fact that a single observable, the fluorescent signal of the ANS, is being fit to at least six variables in a mechanism involving two intermediates. Accurate global fits require a higher ratio of observable species to variables to be meaningful. For example, the three different rates could be due to different binding environments within the cavity. Then the final rate was the convergence to a single binding site resembling that seen in the crystal. Fitting of this mechanism, however, would require the fluorescent coefficients of the intermediate species, which are unknown.

The observed rates nevertheless indicate a process that behaves similarly to the expected pseudo-first-order behavior of a simple binding reaction. This is additive with two other processes. The first process is dependent on ligand

concentration, an order of magnitude slower than the binding reaction. The second process appears independent of ligand concentration, and occurs at $\sim 1\ s^{-1}$. Further analysis of this reaction using mutants of ALBP suspected to have different ligand binding kinetics [such as V32D/F57H (Ory et al., 1997)] are needed to better characterize this complex system.

In the kinetics of IFABP binding, a concentration-independent process was also seen, which was fit to a structural isomerization between an open and closed state of the protein (Cistola et al., 1996). The rate of isomerization was $1000\ s^{-1}$, while the process in the ALBP reaction is $1\ s^{-1}$. This can be reconciled when two things are taken into account: 1) the IFABP experiments were performed at 25°C, and the ALBP at 4°C, and 2) ^{15}N relaxation experiments on apo forms of ALBP and IFBAP suggest IFABP is more flexible than ALBP (Constantine et al., 1998; Hodsdon and Cistola, 1997).

To further test and explore the idea of protein flexibility in the binding reaction, all crystal structures of native ALBP solved to date, including the ANS bound structures, were aligned using LSQMAN (Kleywegt and Jones, 1994), and analyzed as an ensemble of structures. The results are presented as a MOLMOL (Koradi et al., 1996) sausage diagram in Fig. 6. The deviations in conformation are much smaller because they are all crystal structures, and almost all the entries were refined from the same initial structure. However, some interesting variations are found. As is clearly seen in Fig. 6, the areas that deviate in main chain conformation among the nine structures are localized to the βC-βD turn and helix αII. These same areas are found to be disordered on the microsecond-to-picosecond time scale according to ^{15}N relaxation experiments carried out with apo form ALBP (Constantine et al., 1998).

It is unclear whether disorder on this time scale can be correlated with the more discrete disorder seen in apo IFABP structure (Hodsdon and Cistola, 1997). However, this lends further credence to the concept of these areas being flexible, as presumably variations in structure found by crystallography are of a smaller order of magnitude due to crystal packing forces than those found in well-resolved NMR structures.

In summary, ANS provides a novel way to measure dissociation constants using fluorescent methods and competition with physiological ligands such as fatty acids. The crystal structure of the complex demonstrates the nature of the competition. ANS is bound to an overlapping region of the binding cavity seen to interact with fatty acids, but not in the manner expected. The majority of the binding energy derives from enthalpic effects apparently due to favorable nonpolar interactions in the binding cavity. Surprisingly few ionic interactions between ANS and the protein are seen, the only obvious one being a weak interaction between R126 and an oxygen atom of the sulfonate headgroup. A minimum of 10 contacts (3.5–4.5 Å) with nonpolar atoms is made in the crystal structure. Hence, despite the presence of water within the cavity, the fluoroprobe is clearly not experiencing the same environment as it would in the bulk solvent. This change in the surrounding environment is most likely responsible for the fluorescent enhancement. The kinetics of the binding reaction as followed by fluorescent changes is complex, with two processes being additive with the expected pseudo-first-order binding reaction.

FIGURE 6 Flexibility of ALBP crystal structures. A MOLMOL sausage diagram (Koradi et al., 1996) of all native crystal structures of ALBP found in the structural database, including the ALBP/ANS complex. Thicker main chain radii indicate areas of greater deviation. The region surrounding the βC-βD turn is often referred to as the "portal region" defining the most common entry point for ligand binding.

We gratefully acknowledge members of Dr. John Lipscomb's lab in the Department of Biochemistry for the use and assistance with the stopped-flow experiments, especially Brad Wallar. We also to thank Judy Bratt for assistance in purification of ALBP and Ed Hoeffner for maintaining the x-ray generators and computing equipment. We thank members of Dr. Frank Prendergast's lab at the Mayo Clinic, especially Elizabeth Kurian, for their discussions on ANS fluorescence. Finally, members of the Banaszak and Bernlohr laboratories are acknowledged for their useful and insightful discussions.

This study was supported by National Institutes of Health Grant GM 13925. The Minnesota Supercomputer Institute is acknowledged for grant support necessary to refine this structure.

REFERENCES

Banaszak, L., N. Winter, Z. Xu, D. A. Bernlohr, S. Cowan, and T. A. Jones. 1994. Lipid-binding proteins: a family of fatty acid and retinoid transport proteins. *Adv. Protein Chem.* 45:89–151.

Brunger, A. T. 1988. Crystallographic refinement by simulated annealing. Application to a 2.8 Å resolution structure of aspartate aminotransferase. *J. Mol. Biol.* 203:803–816.

Brunger, A. T. 1992. The free R value: a novel statistical quantity for assessing the accuracy of crystal structures. *Nature.* 355:472–474.

Brunger, A. T., J. Kuriyan, and M. Karplus. 1987. Crystallographic R factor refinement by molecular dynamics. *Science.* 235:458–460.

Carter, C. W. J., and C. W. Carter. 1979. Crystallization using incomplete factorial experiments. *J. Biol. Chem.* 254:12219–12223.

Cistola, D. P., K. Kim, H. Rogl, and C. Frieden. 1996. Fatty acid interactions with a helix-less variant of intestinal fatty acid-binding protein. *Biochemistry.* 35:7559–7565.

Constantine, K. L., M. S. Friedrichs, M. Wittekind, H. Jamil, C. H. Chu, R. A. Parker, V. Goldfarb, L. Mueller, and B. T. Farmer II. 1998. Backbone and side chain dynamics of uncomplexed human adipocyte and muscle fatty acid-binding proteins. *Biochemistry.* 37:7965–7980.

Dang, Q., and C. Frieden. 1997. New PC versions of the kinetic-simulation and fitting programs, KINSIM and FITSIM. *Trends Biochem. Sci.* 22: 317.

Hodsdon, M. E., and D. P. Cistola. 1997. Discrete backbone disorder in the nuclear magnetic resonance structure of apo intestinal fatty acid-binding protein: implications for the mechanism of ligand entry. *Biochemistry.* 36:1450–1460.

Jancarik, J., and S. H. Kim. 1991. Sparse matrix sampling: a screening method for crystallization of proteins. *J. Appl. Crystallogr.* 24:409–411.

Jiang, J. S., and A. T. Brunger. 1994. Protein hydration observed by x-ray diffraction. Solvation properties of penicillopepsin and neuraminidase crystal structures. *J. Mol. Biol.* 243:100–115.

Johnson, J. D., M. A. El-Bayoumi, L. D. Weber, and A. Tulinsky. 1979. Interaction of alpha-chymotrypsin with the fluorescent probe 1- anilinonaphthalene-8-sulfonate in solution. *Biochemistry.* 18:1292–1296.

Kane, C. D., and D. A. Bernlohr. 1996. A simple assay for intracellular lipid-binding proteins using displacement of 1-anilinonaphthalene 8-sulfonic acid. *Anal. Biochem.* 233:197–204.

Kirk, W. R., E. Kurian, and F. G. Prendergast. 1996. Characterization of the sources of protein-ligand affinity: 1-sulfonato-8-(1′)anilinonaphthalene binding to intestinal fatty acid binding protein. *Biophys. J.* 70: 69–83.

Kleywegt, G. J., and T. A. Jones. 1994. VOIDOO reference. *Acta. Crystallogr. D.* 50:178–185.

Koradi, R., M. Billeter, and K. Wuthrich. 1996. MOLMOL: a program for display and analysis of macromolecular structures. *J. Mol. Graphics.* 14:51–55, 29–32.

Kurian, E., W. R. Kirk, and F. G. Prendergast. 1996. Affinity of fatty acid for rat intestinal fatty acid binding protein: further examination. *Biochemistry.* 35:3865–3874.

LaLonde, J. M., D. A. Bernlohr, and L. J. Banaszak. 1994a. X-ray crystallographic structures of adipocyte lipid-binding protein complexed with palmitate and hexadecanesulfonic acid. Properties of cavity binding sites. *Biochemistry.* 33:4885–4895.

LaLonde, J. M., M. A. Levenson, J. J. Roe, D. A. Bernlohr, and L. J. Banaszak. 1994b. Adipocyte lipid-binding protein complexed with arachidonic acid. Titration calorimetry and x-ray crystallographic studies. *J. Biol. Chem.* 269:25339–25347.

Liang, J., H. Edelsbrunner, and C. Woodward. 1998. Anatomy of protein pockets and cavities: measurement of binding site geometry and implications for ligand design. *Protein Sci.* 7:1884–1897.

LiCata, V., and D. Bernlohr. 1998. Surface properties of adipocyte lipid-binding protein: response to lipid binding and comparison with homologous proteins. *Proteins.* 33:577–589.

McDonald, I. K., and J. M. Thornton. 1994. Satisfying hydrogen bonding potential in proteins. *J. Mol. Biol.* 238.

Ory, J., C. D. Kane, M. A. Simpson, L. J. Banaszak, and D. A. Bernlohr. 1997. Biochemical and crystallographic analyses of a portal mutant of the adipocyte lipid-binding protein. *J. Biol. Chem.* 272:9793–9801.

Ory, J. J., A. Mazhary, H. Kuang, R. R. Davies, M. D. Distefano, and L. J. Banaszak. 1998. Structural characterization of two synthetic catalysts based on adipocyte lipid binding protein. *Protein Eng.* 11:253–261.

Slavik, J., J. Horak, L. Rihova, and A. Kotyk. 1982. Anilinonaphthalene sulfonate fluorescence and amino acid transport in yeast. *J. Membr. Biol.* 64:175–179.

Tonomura, B., H. Nakatani, M. Ohnishi, J. Yamaguchi-Ito, and K. Hiromi. 1978. Test reactions for a stopped-flow apparatus. Reduction of 2,6-dichlorophenolindophenol and potassium ferricyanide by L-ascorbic acid. *Anal. Biochem.* 84:370–383.

Weber, L., A. Tulinsky, J. Johnson, and M. El-Bayoumi. 1979. Expression of functionality of alpha-chymotrypsin. The structure of a fluorescent probe-alpha-chymotrypsin complex and the nature of its pH dependence. *Biochemistry.* 18:1297–1303.

Xu, Z. H., M. K. Buelt, L. J. Banaszak, and D. A. Bernlohr. 1991. Expression, purification, and crystallization of the adipocyte lipid binding protein. *J. Biol. Chem.* 266:14367–14370.